

SCIENTIFIC REPORTS



OPEN

Tunable critical temperature for superconductivity in FeSe thin films by pulsed laser deposition

Zhongpei Feng^{1,2}, Jie Yuan^{1,2}, Ge He^{1,2}, Wei Hu^{1,2}, Zefeng Lin^{1,2}, Dong Li^{1,2}, Xingyu Jiang^{1,2}, Yulong Huang^{1,2}, Shunli Ni^{1,2}, Jun Li³, Beiyi Zhu¹, Xiaoli Dong^{1,2}, Fang Zhou^{1,2}, Huabing Wang³, Zhongxian Zhao^{1,2,4} & Kui Jin^{1,2,4}

Stabilized FeSe thin films in ambient pressure with tunable superconducting critical temperature would be a promising candidate for superconducting electronic devices. By carefully controlling the depositions on twelve kinds of substrates using a pulsed laser deposition technique single crystalline FeSe thin films were fabricated. The high quality of the thin films was confirmed by X-ray diffraction with a full width at half maximum of 0.515° in the rocking curve and clear four-fold symmetry in φ -scan. The films have a maximum $T_c \sim 15$ K on the CaF_2 substrate and were stable in ambient conditions air for more than half a year. Slightly tuning the stoichiometry of the FeSe targets, the superconducting critical temperature becomes adjustable below 15 K with quite narrow transition width less than 2 K. These FeSe thin films deposited on different substrates are optimized respectively. The T_c of these optimized films show a relation with the out-of-plane (*c*-axis) lattice parameter of the FeSe films.

The Fe-based superconductors have attracted a lot of attention due to their intriguing superconducting properties and their promise towards novel applications^{1,2}. Among various Fe-based superconductors, the 11-system possesses the simplest structure as the anti-PbO-type structure (space group of $P4/nmm$)^{3,4} but displays the most multifarious physical properties in all Fe-based superconductors. The 11-system includes the $\text{FeSe}_{1\pm x}$ ^{5,6}, $\text{Fe}_{1\pm y}(\text{Se},\text{Te})$ ^{7,8} and $\text{Fe}_{1\pm y}(\text{Se},\text{S})$ ⁹, among which the FeSe deserves more attentions. The FeSe bulk crystals exhibit an onset superconducting critical temperature (T_c) of 9 K in ambient pressure⁵, which can be enhanced up to 38 K under external pressure. This effect is attributed to a decrease of anion height from the Fe-square planes, highlighting the impact of crystal lattice on superconductivity^{10–14}. Unexpectedly, the T_c can be enhanced to 65 K for one unit cell (UC) of FeSe on SrTiO_3 substrate^{15–21}. Because of the extreme sensitivity to oxygen, such ultra-thin films of one or a few UC can only be investigated by combining *in-situ* fabrication and characterization. This drastically limits the possibilities to conduct research or develop novel applications based on this intriguing material. Therefore, more stable FeSe films, comparable to or even better than the bulk crystals, are highly desired for the next generation of Fe-based superconducting electronic devices.

The fabrication of FeSe thin films has been widely studied using pulsed laser deposition (PLD)^{2,6,22–27} and molecular beam epitaxy (MBE)^{2,15–21,28,29}. From application point of view, PLD is much more efficient for the growth of films with moderate thickness (above 100 nm). The FeSe can be grown on various substrates, such as LaAlO_3 , SrTiO_3 and MgO , but the obtained T_c values are generally equal to or lower than the T_c of bulk crystals. A recent report showed that CaF_2 substrates could enhance T_c up to 15 K for FeSe films with a thickness of 150 nm²⁷. The strain, induced by mismatch between the substrate and the film, may play a role in promoting T_c ²⁵. However, it usually takes effect within limited film thickness, plausibly for the ultra-thin FeSe films where the T_c decreases quickly from 1 UC to 3 UC¹⁸. As such, it is still an open question why the T_c is enhanced in these thick films. Besides strain^{23,25,29}, other effects, such as modification of the out-of-plane lattice parameter¹³, sample inhomogeneity by Fe vacancies^{30–33}, as well as the growth conditions²⁸, could also influence the superconducting

¹Beijing National Laboratory for Condensed Matter Physics, Institute of Physics, Chinese Academy of Sciences, Beijing, 100190, China. ²Key Laboratory of Vacuum Physics, School of Physical Sciences, University of Chinese Academy of Sciences, Beijing, 100049, China. ³Research Institute of Superconductor Electronics, Nanjing University, Nanjing, 210093, China. ⁴Collaborative Innovation Center of Quantum Matter, Beijing, 100190, China. Correspondence and requests for materials should be addressed to J.Y. (email: yuanjie@iphy.ac.cn) or J.L. (email: junli@nju.edu.cn) or K.J. (email: kuijin@iphy.ac.cn)

Substrate	Crystal Plane	Atomic Distance at Surface (Å)	Mismatch (%)	T_c -onset (K)
CaF ₂	(0 0 1)	$a_0 \times \sqrt{2}/2 = 3.8679$	2.60	15.17
LiF	(0 0 1)	$a_0 = b_0 = 4.0270$	6.82	14.01
SrTiO ₃	(0 0 1)	$a_0 = b_0 = 3.9050$	3.58	11.99
MgO	(0 0 1)	$a_0 = b_0 = 4.2110$	11.70	9.23
BaF ₂	(0 0 1)	$a_0 \times \sqrt{2}/2 = 4.6810$	24.16	9.24
TiO ₂	(1 0 0)	$b_0 = 4.2110, c_0 = 2.9580$	21.83, 21.54	7.86
LaAlO ₃	(0 0 1)	$a_0 = b_0 = 3.720$	0.58	6.41
MgF ₂	(0 0 1)	$a_0 = b_0 = 4.6200$	22.55	5.51
Nb:SrTiO ₃	(0 0 1)	$a_0 = b_0 = 3.9050$	3.58	5.20
LSAT	(0 0 1)	$a_0 = b_0 = 3.8680$	2.60	4.75
(La,Sr)AlO ₃	(0 0 1)	$a_0 = b_0 = 3.7560$	0.37	6.93
MgAl ₂ O ₄	(0 0 1)	$a_0 = b_0 = 8.0830$	7.20	5.96

Table 1. Structure parameters of various substrates.

properties. To solve this intriguing scientific puzzle, it is important to systematically study the crystal lattice and superconducting properties of FeSe films on various substrates.

In this work, we report on the successful synthesis of a series of high-quality single crystalline superconducting FeSe films on various substrates by PLD, with a maximum T_c up to 15 K. Besides, different growth parameters such as the ratio of Fe to Se in the targets and the thickness of the films are also elaborately tuned to arrive at a broad range of T_c . Based on abundant high quality and stabilized samples, the relation between the crystal lattice and the tunable T_c has been carefully studied.

Results

First, all the films on various substrates were grown with the same thickness of ~160 nm for a better comparison, as well as to release the epitaxial strain. The twelve substrates, explored in this work, are CaF₂ (CF), SrTiO₃ (STO), LiF (LF), MgO (MO), BaF₂ (BF), TiO₂(100) (TO), LaAlO₃ (LAO), MgF₂ (MF), Nb-doped SrTiO₃ (NSTO), La_{0.3}Sr_{0.7}Al_{0.65}Ta_{0.35}O₃ (LSAT), (Sr,La)AlO₄ (SLAO), and MgAl₂O₄ (MAO). The material information of these substrates is summarized in Table 1. Figure 1(a,b) show the X-ray diffraction (XRD) data for the FeSe thin films grown on these substrates. All XRD θ - 2θ scan patterns show a high quality (00 l) orientated growth. The measured (002) peaks, shown in Fig. 1(c) and plotted as a function of the measured critical temperature, display a slightly leftward shift with increasing T_c . The c -axis lattice parameters were calculated from XRD θ - 2θ scan data by the Bragg's law, and the results will be discussed in the latter part. The full width at half maximum (FWHM) of the XRD rocking curve is 0.515°, showing high crystalline quality. In addition, the high quality epitaxy of the different films is confirmed by a clear four-fold symmetry in the XRD φ scan pattern for the (011) diffraction peak, as shown in Fig. 1(e).

Figure 2 shows the temperature dependence of the resistance (R - T) curves for all fabricated films. Since the fabrication process is identical, the superconducting properties strongly depend on the substrates. In most samples, a zero-resistance transition can be observed except the films on the substrates of MAO and LSAT, for which a low- T upturn occurs in the R - T curves above 2 K. Comparing the films deposited on all substrates, the FeSe/CF films are selected for further exploration, since the T_c is the highest in this work.

Since the thickness is considered as a key factor for superconductivity of thin films^{22,23,25,29}, especially the ultra-thin FeSe system^{15,18,29}, we also studied the thickness dependence of T_c for the FeSe/CF films. The films with different thicknesses were prepared by only adjusting the pulsed laser counts, while keeping the same FeSe_{0.95} target. In Fig. 3(a), we show the R - T curves for the FeSe films with different thicknesses. Superconductivity still remains as the thickness is reduced to 20 nm and 10 nm (about 36 and 18 UC) respectively, where $T_{c0} = 3.4$ K and 2 K, indicating the high quality of our FeSe films with less disorder and the stability of our PLD chamber. Increasing film thickness, the T_c also ascends gradually and the films almost display a bulk-like behavior when the thickness exceeds 160 nm.

In previous work, the superconductivity of FeSe films is found to be extremely sensitive to the stoichiometry between Fe and Se³⁰. Therefore, considering the composition off-stoichiometry for the superconductivity of FeSe films, namely the vacancies or interstitial impurity^{30,32}, we prepared the targets with subtle adjustment in the nominal Fe:Se, including 1:1.10, 1:1.05, 1:1.03, 1:1.00, 1:0.99, 1:0.97, 1:0.95, 1:0.90, and so on. For comparison, the films were grown with the same thickness of ~160 nm and on the same CF substrate. Figure 3(b) shows the R - T curves for films grown from different targets. The T_c of the films can be well tuned from < 2 K to 15 K with a pretty narrow transition width ($\Delta T < 2$ K). It should be noted that the best sample deposited by the FeSe_{0.97} target shows that $\Delta T = 1.2$ K, RRR = 5, $T_c = 15$ K, which can hold for more than half a year. By precise adjustment of the nominal composition, it seems that the ratio of Fe:Se is closely related to the superconductivity of the deposited films. Both energy dispersive X-ray spectra (EDX) and inductively coupled plasma atomic emission spectroscopy (ICP-AES) have been used to check the chemical composition. However, the composition between different superconducting films cannot be clearly defined by these two methods. Thus, we prefer to study on the stoichiometry of Fe and Se on the target rather than on the FeSe thin films themselves.

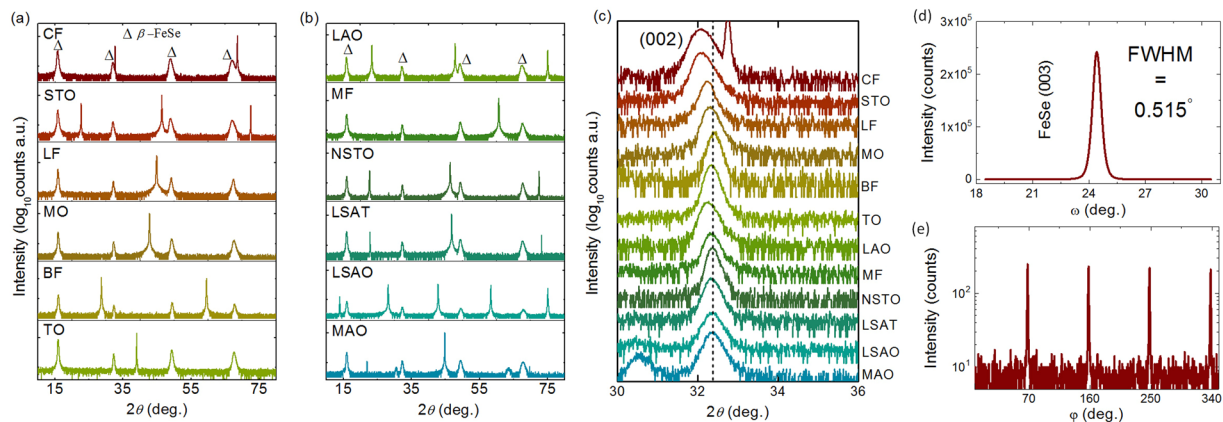


Figure 1. X-ray diffraction data of FeSe thin films. **(a,b)** The XRD θ - 2θ scan data for FeSe thin films on various substrates. The triangles mark the Bragg diffraction peaks. The order is CaF₂ (CF) SrTiO₃ (STO), LiF (LF), MgO (MO), BaF₂ (BF), TiO₂ (100) (TO), LaAlO₃ (LAO), MgF₂ (MF), Nb-doped SrTiO₃ (NSTO), La_{0.3}Sr_{0.7}Al_{0.65}Ta_{0.35}O₃ (LSAT), (Sr,La)AlO₄ (SLAO), and MgAl₂O₄ (MAO). **(c)** The enlarged view of the FeSe(002) peaks. These peaks exhibit obvious shift for different substrates. Here, the dash line is related to the (002) peak of FeSe/MAO. **(d)** The XRD rocking curve data of FeSe/CaF₂. **(e)** The XRD φ -scan data of FeSe/CaF₂. A four-fold symmetry of FeSe(011) diffraction peak indicates a high-quality epitaxial growth.

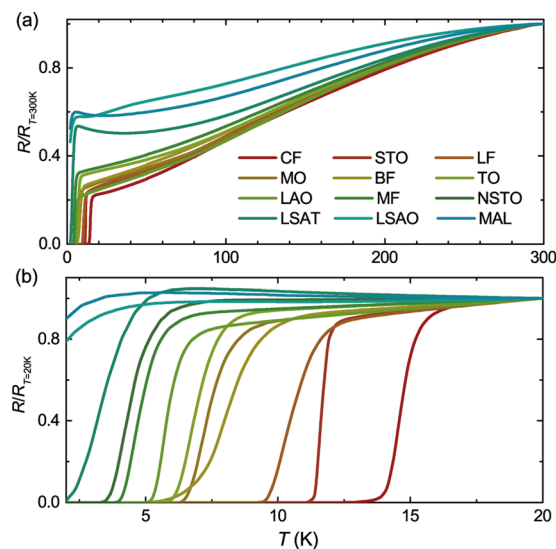


Figure 2. Temperature dependence of normalized resistance R/R_N for FeSe thin films with respect to various substrates. Here, R_N corresponds to the resistance at 300 K and 20 K for **(a)** and **(b)**, respectively, and the thickness of all films are \sim 160 nm.

Discussion

Figure 4(a) gives the T_{c0} (zero resistance superconducting critical temperature) with respect of the corresponding lattice constant c of FeSe films deposited on various substrates. The T_{c0} shows a clear positive correlation with the lattice constant c (the dashed line is a guide to the eye), rather than the in-plane lattice parameter (d) of the substrates (Fig. 4(b)), indicating the epitaxial strain from substrate has been released in films with thickness of 160 nm. In FeSe/TO films the substrate can induce an anisotropic epitaxial strain, because of the rectangular lattice on the surface of the TO substrate ($b = 4.593 \text{ \AA}$, $c = 2.958 \text{ \AA}$). However, the FeSe/TO films display a T_{c0} of 5.6 K, which is still comparable to that of certain films with isotropic strain. Therefore, the c -axis lattice constant is more closely related to the superconductivity of FeSe thin films. Comparably, the superconductivity of the multi-layered FeSe-based superconductors, i.e., (Li_{1-x}Fe_x)OHFeSe³⁴ and Fe(Se_{0.5}Te_{0.5})³⁵, shows a similar c -axis constant dependence behavior, which reinforces our understanding on the profile of lattice parameters to the superconductivity. The c -axis lattice parameter depends on the anion height from the Fe layer^{4,36,37} (or the bond angle of Se-Fe-Se^{4,38}) and the distance between two adjacent Fe₂Se₂ layer³⁹, which will influence the magnetism and interlayer coupling respectively. Therefore, it deserves more in-depth study to uncover the internal mechanism for this positive correlation between T_c and lattice constant c .

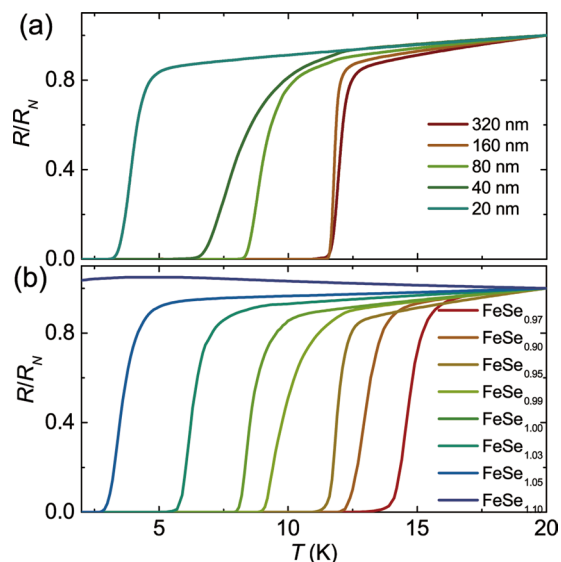


Figure 3. The normalized resistance vs. temperature (R/R_N - T) curves for FeSe/CaF₂ thin films with respect to thicknesses and targets. Here, the R_N was defined as the resistance at 20 K. **(a)** A series of FeSe/CaF₂ films with various thicknesses are fabricated by only adjusting the laser pulsed counts. Here, all films were deposited at 350 °C by using the same target (Fe:Se = 1:0.95). **(b)** The FeSe/CaF₂ films are grown from different targets in a range of Fe:Se ratio from 1:1.10 to 1:0.90, in which the film deposited from the Fe:Se = 1:0.97 target is observed the highest T_c . The order of films fabricated by different FeSe_{1±x} targets is arranged along T_c increasing, namely, from FeSe_{1.10} to FeSe_{1.05}, FeSe_{1.03}, FeSe_{1.00}, FeSe_{0.99}, FeSe_{0.95}, FeSe_{0.90}, and FeSe_{0.97}.

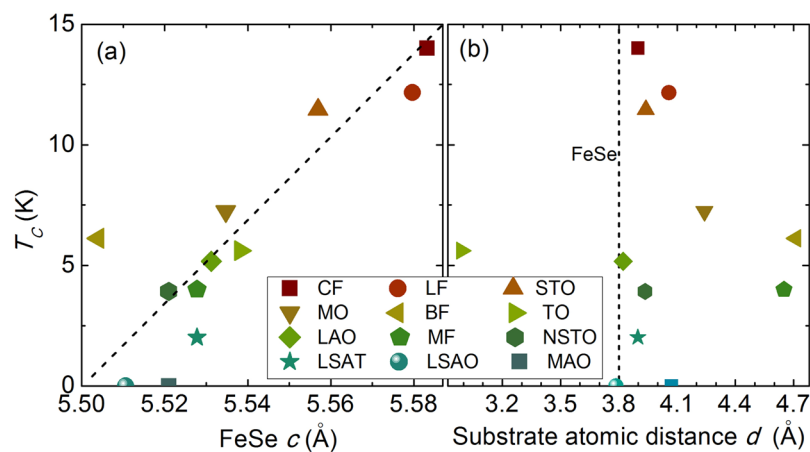


Figure 4. Lattice parameters dependence of superconductivity for FeSe thin films on various substrates. **(a)** T_{c0} versus c (FeSe lattice constant); **(b)** T_{c0} versus d (substrate atomic distance).

In summary, we have successfully prepared high quality superconducting FeSe films on twelve different substrate type, such as CF, LF, STO, LAO, TO, MO, BF, MF, NSTO, LSAT, SLAO and MAO. Among them, the FeSe films deposited on CF, LF and STO substrates possess the highest values of T_c for 15 K, 14 K and 12 K, respectively. By slightly adjusting the ratio of Fe to Se in the targets, a series of FeSe/CF films with tunable T_c values from < 2 K to 15 K are obtained. The superconductivity of the films (~160 nm) on various substrates is found to be mainly correlated with the c -axis lattice parameter of FeSe films. However, there is no direct correlation between the T_c and the surface atomic distance of substrates. The origin of the modification on c -axis parameter needs to be further identified, nevertheless, high-quality FeSe thin films with tunable T_c may pave the way for understanding the nature of FeSe from bulk crystal to ultrathin films, and shed light on the applications of superconducting micro-electronic devices, such as the hybrid Josephson junctions, single-photon detection superconducting nanowires, and so on.

Methods

FeSe polycrystalline targets were fabricated by the solid-state reaction method. The original materials of Fe (4N, Alfa Aesar Inc.) and Se (5N, Alfa Aesar Inc.) powders were mixed with designed ratio of stoichiometry, then

heat-treated at 420 °C for 24 hours in evacuated quartz tubes. The as-prepared material was grinded and sintered at 450 °C for 48 hours, and such process was repeated more than three times for final targets. FeSe thin films were prepared by PLD technique with a KrF laser. The background vacuum of the deposition chamber is better than 10^{-7} Torr. The FeSe thin films were grown in vacuum with the target-substrate distance of ~ 50 mm, the laser energy of 350 mJ, the laser repetition of 2 Hz, and the substrate temperature of 350 °C. And then, the real deposition rate can be fixed at 1.3 nm/min.

X-ray diffraction (XRD) and X-ray reflection (XRR) measurements of the thin films were performed on a Rigaku SmartLab (9 kW) X-ray diffractometer with Ge(220) \times 2 crystal monochromator. The Scanning Electron Microscope (SEM) measurements of the thin films were performed on a Hitachi Scanning electron microscope SU5000. In this work, for the thin films with thickness less than 80 nm, we check the thickness by both XRR and SEM. However, for the film thickness more than 80 nm, we will check them by SEM only. The transport properties of films were measured in the Physical Property Measurement System (PPMS-9 T).

References

- Kamihara, Y. *et al.* Iron-based layered superconductor $\text{La}[\text{O}_{1-x}\text{F}_x]\text{FeAs}$ ($x = 0.05\text{--}0.12$) with $T_c = 26$ K. *J. Am. Chem. Soc.* **130**, 3296 (2008).
- Haindl, S. *et al.* Thin film growth of Fe-based superconductors: from fundamental properties to functional devices. A comparative review. *Rep. Prog. Phys.* **77**, 046502 (2014).
- Paglione, J. & Greene, R. L. High-temperature superconductivity in iron-based materials. *Nat. Phys.* **6**, 645–658 (2010).
- Chen, X. H. *et al.* Iron-based high transition temperature superconductors. *National Science Review* **1**, 371–395 (2014).
- Hsu, F. C. *et al.* Superconductivity in the PbO-type structure α -FeSe. *P. Natl. Acad. Sci. USA* **105**(38), 14262–14264 (2008).
- Han, Y. *et al.* Preparation and superconductivity of iron selenide thin films. *J. Phys. Condens. Matter.* **21**(23), 235702 (2009).
- Fang, M. H. *et al.* Superconductivity close to magnetic instability in $\text{Fe}(\text{Se}_{1-x}\text{Te}_x)_{0.82}$. *Phys. Rev. B.* **78**, 224503 (2008).
- Imai, Y. *et al.* Control of structural transition in $\text{FeSe}_{1-x}\text{Te}_x$ thin films by changing substrate materials. *Sci. Rep.* **7**, 46653 (2017).
- Hosoi, S. *et al.* Nematic quantum critical point without magnetism in $\text{FeSe}_{1-x}\text{S}_x$ superconductors. *P. Natl. Acad. Sci. USA* **113**(29), 8139–8143 (2016).
- Böhmer, A. E. *et al.* Lack of coupling between superconductivity and orthorhombic distortion in stoichiometric single-crystalline FeSe. *Phys. Rev. B.* **87**, 180505(R) (2013).
- Kasahara, S. *et al.* Field-induced superconducting phase of FeSe in the BCS-BEC cross-over. *P. Natl. Acad. Sci. USA* **111**(46), 16309–16313 (2014).
- Mizuguchi, Y. *et al.* Superconductivity at 27 K in tetragonal FeSe under high pressure. *Appl. Phys. Lett.* **93**(15), 152505 (2008).
- Medvedev, S. *et al.* Electronic and magnetic phase diagram of β - $\text{Fe}_{1.01}\text{Se}$ with superconductivity at 36.7 K under pressure. *Nat. Mater.* **8**, 630–633 (2009).
- Sun, J. P. *et al.* Dome-shaped magnetic order competing with high-temperature superconductivity at high pressures in FeSe. *Nat. Commun.* **7**, 12146 (2016).
- Wang, Q. Y. *et al.* Interface-induced high-temperature superconductivity in single unit-cell FeSe films on SrTiO_3 . *Chin. Phys. Lett.* **29**(3), 037402 (2012).
- Liu, D. *et al.* Electronic origin of high-temperature superconductivity in single-layer FeSe superconductor. *Nat. Commun.* **3**, 931 (2012).
- He, S. L. *et al.* Phase diagram and electronic indication of high-temperature superconductivity at 65 K in single-layer FeSe films. *Nat. Mater.* **12**, 605–610 (2013).
- Tan, S. Y. *et al.* Interface-induced superconductivity and strain-dependent spin density waves in FeSe/ SrTiO_3 thin films. *Nat. Mater.* **12**, 634–640 (2013).
- Peng, R. *et al.* Tuning the band structure and superconductivity in single-layer FeSe by interface engineering. *Nat. Commun.* **5**, 5044 (2014).
- Ge, J. F. *et al.* Superconductivity above 100 K in single-layer FeSe films on doped SrTiO_3 . *Nat. Mater.* **14**, 285–289 (2015).
- Lee, J. J. *et al.* Interfacial mode coupling as the origin of the enhancement of T_c in FeSe films on SrTiO_3 . *Nature* **515**, 245–248 (2014).
- Wang, M. J. *et al.* Crystal orientation and thickness dependence of the superconducting transition temperature of tetragonal FeSe_{1-x} thin films. *Phys. Rev. Lett.* **103**, 117002 (2009).
- Nie, Y. F. *et al.* Suppression of superconductivity in FeSe films under tensile strain. *Appl. Phys. Lett.* **94**(24), 242505 (2009).
- Chen, T. K. *et al.* Low-temperature fabrication of superconducting FeSe thin films by pulsed laser deposition. *Thin Solid Films* **519**(5), 1540–1545 (2010).
- Nabeshima, F. *et al.* Enhancement of the superconducting transition temperature in FeSe epitaxial thin films by anisotropic compression. *Appl. Phys. Lett.* **103**(17), 172602 (2013).
- Maeda, A. *et al.* Synthesis, characterization, Hall effect and THz conductivity of epitaxial thin films of Fe chalcogenide superconductors. *Appl. Surf. Sci.* **312**, 43–49 (2014).
- Imai, Y. *et al.* Superconducting properties of $\text{FeSe}_{1-x}\text{Te}_x$ films with $x = 0\text{--}0.4$. *Phys. C* **530**, 24–26 (2016).
- Agatsuma, S. *et al.* MBE growth of FeSe and $\text{Sr}_{1-x}\text{K}_x\text{Fe}_2\text{As}_2$. *Phys. C* **470**(20), 1468–1472 (2010).
- Song, C. L. *et al.* Molecular-beam epitaxy and robust superconductivity of stoichiometric FeSe crystalline films on bilayer graphene. *Phys. Rev. B.* **84**, 020503 (2011).
- McQueen, T. M. *et al.* Extreme sensitivity of superconductivity to stoichiometry in Fe_{1+x}Se . *Phys. Rev. B.* **79**, 014522 (2009).
- Schneider, R. *et al.* Superconductor-insulator quantum phase transition in disordered FeSe thin films. *Phys. Rev. Lett.* **108**, 257003 (2012).
- Chen, T. K. *et al.* Fe-vacancy order and superconductivity in tetragonal β - Fe_{1-x}Se . *P. Natl. Acad. Sci. USA* **111**(1), 63–68 (2014).
- Fang, Y. *et al.* Tunable Fe-vacancy disorder-order transition in FeSe thin films. *Phys. Rev. B.* **93**, 184503 (2016).
- Dong, X. L. *et al.* Phase diagram of $(\text{Li}_{1-x}\text{Fe}_x)\text{OHFeSe}$: A bridge between iron selenide and arsenide superconductors. *J. Am. Chem. Soc.* **137**, 66 (2015).
- Imai, Y. *et al.* Superconductivity of $\text{FeSe}_{0.5}\text{Te}_{0.5}$ thin films grown by pulsed laser deposition. *Jpn. J. Appl. Phys.* **49**, 023101 (2010).
- Mizuguchi, Y. *et al.* Anion height dependence of T_c for the Fe-based superconductor. *Supercond. Sci. Technol.* **23**, 054013 (2010).
- Lu, X. F. *et al.* Superconductivity in $\text{LiFeO}_2\text{Fe}_2\text{Se}_2$ with anti-PbO-type spacer layers. *Phys. Rev. B.* **89**, 020507 (R) (2013).
- Lee, C. H. *et al.* Relationship between crystal structure and superconductivity in iron-based superconductors. *Solid State Commun.* **152**, 644–648 (2012).
- Noji, T. *et al.* Synthesis and post-annealing effects of alkaline-metal-ethylenediamine-intercalated superconductors $\text{A}_x(\text{C}_2\text{H}_8\text{N}_2)_y\text{Fe}_2\text{Se}_2$ ($\text{A} = \text{Li, Na}$) with $T_c = 45$ K. *Phys. C* **504**, 8–11 (2014).

Acknowledgements

This work was supported by National Key Basic Research Program of China (No. 2015CB921000, 2016YFA0300301, 2017YFA0302902 and 2017YFA0303003), National Natural Science Foundation of China (No. 11674374, 11474338,

11574372, 11234006, 61771234, and 61501220), the Key Research Program of Frontier Sciences, CAS (No. QYZDY-SSW-SLH001 and QYZDY-SSW-SLH008), Strategic Priority Research Program of CAS (No. XDPB01, XDB07020100 and XDB07030200), Beijing Municipal Science and Technology Project (No. Z161100002116011, D1 61100002416001, D161100002416003), Jiangsu Provincial Natural Science Fund (No. BK20150561), and Opening Project of Wuhan National High Magnetic Field Center (No. 2015KF19).

Author Contributions

Jie Yuan, Xiaoli Dong, Fang Zhou, Zhongxian Zhao and Kui Jin conceived the experiments; Zhongpei Feng, Ge He, Wei Hu, Zefeng Lin, Dong Li, Xingyu Jiang, Yulong Huang and Shunli Ni, conducted the experiments; Zhongpei Feng analysed the results; Jie Yuan, Jun Li, Huabing Wang, Beiyi Zhu, and Kui Jin wrote the paper. All authors have reviewed the manuscript.

Additional Information

Supplementary information accompanies this paper at <https://doi.org/10.1038/s41598-018-22291-z>.

Competing Interests: The authors declare no competing interests.

Publisher's note: Springer Nature remains neutral with regard to jurisdictional claims in published maps and institutional affiliations.



Open Access This article is licensed under a Creative Commons Attribution 4.0 International License, which permits use, sharing, adaptation, distribution and reproduction in any medium or format, as long as you give appropriate credit to the original author(s) and the source, provide a link to the Creative Commons license, and indicate if changes were made. The images or other third party material in this article are included in the article's Creative Commons license, unless indicated otherwise in a credit line to the material. If material is not included in the article's Creative Commons license and your intended use is not permitted by statutory regulation or exceeds the permitted use, you will need to obtain permission directly from the copyright holder. To view a copy of this license, visit <http://creativecommons.org/licenses/by/4.0/>.

© The Author(s) 2018